

Optimal Mismatched Filtering to Address Clutter Spread from Intra-CPI Variation of Spectral Notches

Brandon Ravenscroft¹, Jonathan W. Owen¹, Shannon D. Blunt¹, Anthony F. Martone², Kelly D. Sherbondy²

¹Radar Systems Lab (RSL), University of Kansas, Lawrence, KS

²Sensors and Electron Devices Division, Army Research Laboratory (ARL), Adelphi, MD, USA

Abstract—It was recently shown that cognitive spectral notching of FM noise waveforms on transmit is an effective means with which to avoid relatively narrow in-band interference, such as occurs for radar/communication spectrum sharing. It was likewise observed, however, that when the notch is required to move during the coherent processing interval (CPI) to address dynamic interference, the resulting nonstationarity induces increased residual clutter after cancellation. Here we examine the impact of least-squares based mismatched filtering (MMF) to compensate for this residue. This manner of MMF is required not only to reduce the range sidelobe modulation that arises from dynamic transmit notching, but also to maintain the notch on receive so that the effect of in-band interference is minimized.

Keywords—spectrum sharing, cognitive radar, spectrum notching, mismatched filtering, FM noise radar

I. INTRODUCTION

Accelerating congestion and competition for RF spectrum [1-2] is driving research into the mitigation of narrowband radio frequency interference (RFI) inside radar operating bands [3-9]. Specifically, the push for greater sharing of the spectrum [10] may require that radars strive to avoid causing interference to other spectrum users in addition to the present need to suppress received interference.

To that end, in [9] a cognitive radar framework was introduced and experimentally evaluated in which a rapid band-aggregation technique [11] was used to identify sources of interference operating within a radar spectrum to facilitate the subsequent formation of spectral notches in a set of FM noise waveforms [12]. The benefit of spectrally notching FM noise waveforms is that the increased range sidelobe penalty incurred by notching [13] is far less severe for these non-repeating waveforms because their sidelobes combine incoherently when performing Doppler processing [12].

It was shown in [8-9] that transmit spectral notching (and subsequent matched filtering that is likewise spectrally notched) can significantly reduce the interference caused and received by the radar. The degree of reduction in received interference is tempered, however, when the spectral location of a notch is moved during the CPI for the purpose of addressing dynamic RFI. This limitation takes the form of residual clutter that is smeared across Doppler (see Fig. 1). While the use of non-repeating waveforms does generally involve some modest increase in residual clutter that is spread in range/Doppler as a result of range sidelobe modulation (RSM) (e.g. see [12, 14-16]), this effect by itself does not tend

to be as severe as when spectral notches are moved, because the latter also induces a modulation of the pulse compression mainlobe. That said, in [12,17] it was shown that the use of least-squares (LS) optimal mismatched filtering (MMF) [18], suitably modified to be applicable to FM waveforms [19], can markedly reduce the RSM component of residual clutter.

This paper therefore examines the impact of likewise employing a LS-MMF determined for each unique waveform, albeit with the added caveat of maintaining the spectral notch on receive. The efficacy of this receive filtering strategy is evaluated in simulation relative to the notched matched filter for FM noise waveforms having no notch, a static notch, and a spectrally hopping notch during the CPI. The presence (or not) of the in-band interference is also assessed.

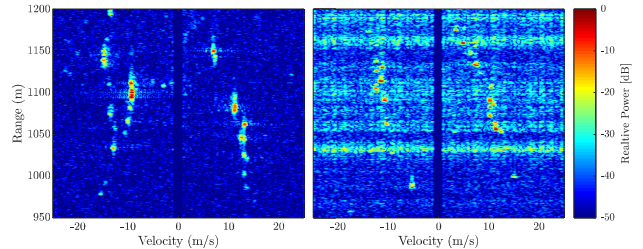


Fig. 1. Free-space measurements of moving targets after clutter cancellation using (left) FM noise waveforms with a static notch and (right) FM noise waveforms with a moving notch. No interference is present.

II. SPECTRALLY NOTCHED FM NOISE WAVEFORMS

These waveforms are continuous in phase and have a constant amplitude. They are designed by discretizing the continuous signal with sufficient over-sampling relative to 3-dB bandwidth such that an adequate portion of the spectrum roll-off is captured, and thus the unavoidable aliasing is minimized to the degree of fidelity needed [20].

The design of each waveform first involves initialization with an independent random FM waveform, which can be readily obtained via the polyphase-coded FM (PCFM) scheme [21]. Various iterative optimization procedures can then be applied to each initial random waveform so that it has relatively low range sidelobes while still remaining unique, which means each waveform also has a unique sidelobe structure. Optimization procedures that have been demonstrated thus far include pseudo-random optimized FM (PRO-FM) [12], which employs alternating projections in time and frequency, gradient descent optimization according to a generalized integrated sidelobe (GISL) metric [22], a

frequency template error (FTE) metric [23], and most recently to a temporal template error (TTE) metric [24]. All of these produce FM waveforms having good spectral containment that are readily amenable for high-power radar transmitters.

Most of the FM noise design approaches impose a desired spectral shape $|G(f)|$ on each waveform. Thus when a spectral notch is required, the spectrum can be modified accordingly as

$$|G(f)| = 0 \text{ for } f \in \Omega, \quad (1)$$

where Ω represents the frequency interval(s) of the notch(es) [9]. Tapering around each frequency interval can also be incorporated to mitigate the $\sin(x)/x$ roll-off in autocorrelation sidelobes that result from sharp notch edges [9].

Introducing (1) in the desired waveform spectrum may not be sufficient to achieve necessary notch depths, however. If so, the reiterative uniform weight optimization (RUWO) method [25] or a recent analytical spectrum notching technique [20] can be applied. Thus far both approaches have experimentally demonstrated notch depths better than -50 dB.

III. LS-MMF FOR NOTCHED FM NOISE WAVEFORMS

Denote the radar waveform as $s(t)$. It has pulse width T and 3-dB bandwidth B . Let K indicate the amount of over-sampling with respect to the 3-dB bandwidth in order to represent the discretized version of $s(t)$ with sufficient fidelity. Denote this discretized version as $\mathbf{s} = [s_1 \ s_2 \ \dots \ s_N]^T$, where $N = K(BT)$ is the length of vector \mathbf{s} .

Per [19, 21], construct the banded Toeplitz matrix

$$\mathbf{A} = \begin{bmatrix} s_1 & 0 & \cdots & 0 \\ \vdots & s_1 & \ddots & \vdots \\ s_N & \vdots & \ddots & 0 \\ 0 & s_N & s_1 & \\ \vdots & & \ddots & \vdots \\ 0 & \cdots & 0 & s_N \end{bmatrix}, \quad (2)$$

which has dimensions $((M+1)N-1) \times MN$, for MN the length of the MMF (2N to 4N typically). The LS-MMF filter is then realized as [19, 21]

$$\mathbf{h}_{\text{MMF}} = (\tilde{\mathbf{A}}^H \tilde{\mathbf{A}} + \sigma \mathbf{I})^{-1} (\tilde{\mathbf{A}}^H \mathbf{e}_m), \quad (3)$$

where σ is a diagonal loading factor, \mathbf{I} is an $MN \times MN$ identity matrix, \mathbf{e}_m is a length $((M+1)N-1)$ elementary vector with a ‘1’ in the m th position (usually near the middle) and zeros elsewhere, and $(\cdot)^H$ is the Hermitian operator.

An important distinction is that the matrix $\tilde{\mathbf{A}}$ in (3) is the same as \mathbf{A} defined in (2) but with the $K-1$ rows above and below the m th row replaced with zeros. As described in [19, 21], this modification provides a “beamspoiling” effect to avoid the degradation that otherwise arises from super-resolution due to \mathbf{s} being over-sampled. While not considered here, alternative formulations involving modification of the \mathbf{e}_m vector have also been explored [12, 17].

Regardless of the particular version of (FM modified) LS-MMF used, each individual waveform in an FM noise CPI requires determination of its own specific filter since each waveform is unique. Further, for utility with spectrally notched waveforms it is necessary that the LS-MMF preserves the

notch so that the RFI is not passed (much less enhanced, which could occur if one is not careful about the MMF design due to the inverse aspect of LS).

As an anecdotal example, Fig. 2 illustrates the root mean squared (RMS) power spectrum of a notched waveform and a LS-MMF constructed in the manner of (3). As with the other results that follow, the value of σ was set to be 2% of the largest eigenvalue of $(\tilde{\mathbf{A}}^H \tilde{\mathbf{A}})$. We see that the MMF realizes a ~ 18 dB shallower notch depth than the matched filter (MF), which is identical to the waveform spectrum. The MMF also exhibits a noticeable “flaring” about the notch that indicates one must be sure the waveform notch has sufficient width to encompass the RFI.

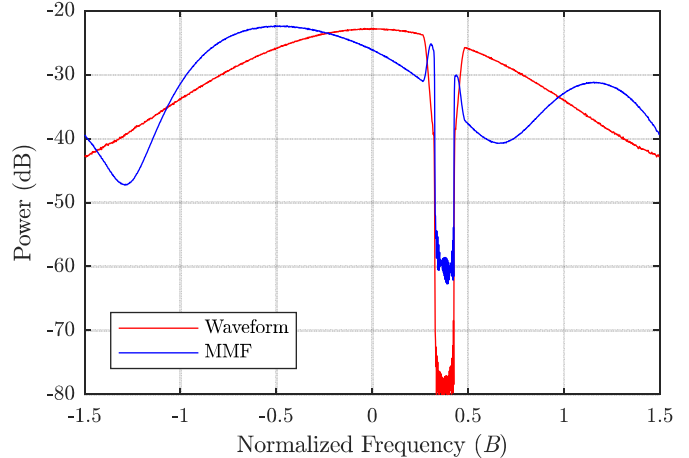


Fig. 2. RMS power spectrum averaged over 1000 notched PRO-FM waveforms and their corresponding LS-MMFs from (3)

IV. SIMULATED ASSESSMENT OF LS-MMF

To assess the efficacy of the LS-MMF of (3) to address increased RSM caused by moving spectral notches, we evaluate in simulation the delay/Doppler point spread function (PSF) obtained from pulse compressing and Doppler processing different CPIs of non-repeating waveforms under the hypothetical condition of a point scatterer. These different CPIs correspond to cases in which 1) no notch is present, 2) a static notch of width $B/10$ is present, and 3) a notch of width $B/10$ moves randomly within the 3-dB bandwidth B after a prescribed time interval. The static notch is near the $+0.5B$ band edge, being centered at a normalized frequency of $+3B/8$. The moving notch changes location after every 10 pulse repetition intervals (PRIs).

For each of the three cases, $P = 1000$ PRO-FM pulsed waveforms [12] are independently generated, with each waveform having a time-bandwidth product of $BT = 200$. Each spectral notch employs Tukey tapering of the notch edges [9] to reduce $\sin(x)/x$ range sidelobes. A LS-MMF is generated for each individual waveform according to (3) using $M = 3$. For each PSF, pulse compression is performed with both the standard MF and LS-MMF, followed by unwindowed Doppler processing across the P pulses in the CPI.

Since the sole purpose for spectral notching is to avoid in-band interference, we consider its impact on each of the three cases above by evaluating the PSF response both with and

without interference present. Here the interference is modeled as a collection of orthogonal frequency division multiplexed (OFDM) subcarriers with an arbitrary 64-QAM symbol modulated onto each subcarrier.

The OFDM signal in each case has a bandwidth of $B/12$ (slightly narrower than the notch width) and the average peak power is set to be 20 dB above the peak power of the corresponding waveform spectrum. Further, the noise floor in this simulated arrangement is set to be 20 dB below the bottom of the notch.

For Case 1 (no notch) and Case 2 (static notch), the OFDM interference is centered at a normalized frequency of $+3B/8$. For Case 3 (hopping notch) the interference and notch synchronously hop in tandem, which presupposes that the interference location can be determined clairvoyantly for notch placement. This condition is clearly not realistic, but it does provide a way to evaluate the best possible performance that could be achieved. In [9] the impact of latency on notch placement was also considered.

A useful PSF-based metric for the comparison of residual clutter due to nonrepeating waveforms can be defined as

$$\delta = \frac{1}{n(L)n(\Omega_D)} \sum_{\ell \in L} \sum_{\omega_D \in \Omega_D} \rho(\ell, \omega_D) \quad (4)$$

for $\ell \neq 0 \pm \Delta\ell, \omega_D \neq 0 \pm \Delta\omega_D$,

where $\rho(\ell, \omega_D)$ is the delay/Doppler PSF, and $\pm\Delta\ell$ and $\pm\Delta\omega_D$ correspond to the delay and Doppler mainlobe widths, respectively. These regions are excluded in (4) because they represent the usual delay/Doppler sidelobe response (and may have large values) while we wish to focus on the rest of the PSF where the impact of RSM occurs. Finally, $n(L)$ and $n(\Omega_D)$ are the cardinality of the sets of delay and Doppler values being summed over. When the LS-MMF is evaluated for each case, the value of δ is determined after the PSF has been peak-normalized (and the associated mismatch loss assessed).

A. Case 1: No Spectral Notch

Figures 3 and 4 show the PSF using the MF and LS-MMF when the set of waveforms contains no spectral notch. It can be directly observed that the delay/Doppler “background” is much lower in the latter case. Specifically, the value of δ computed from (4) for the MF and LS-MMF is -69.5 dB and -85.4 dB, respectively, with the important point being that the latter is roughly 16 dB lower. This result is consistent with the experimental measurements in [12]. The trade-off for this reduction is a mismatch loss penalty of only 0.3 dB.

Figure 5 shows the PSF for the same set of waveforms and the LS-MMF filter, albeit with the inclusion of OFDM RFI that is 20 dB above the “received” radar signal (for a hypothetical point scatterer). The MF result is not shown because it has no appreciable difference. The peak is still visible because $P = 1000$ unique waveforms with $BT = 200$ enables a coherent processing gain of 53 dB. That said, the RFI does dramatically raise the background level to -51.3 dB for the MF and -53.8 dB for the LS-MMF.

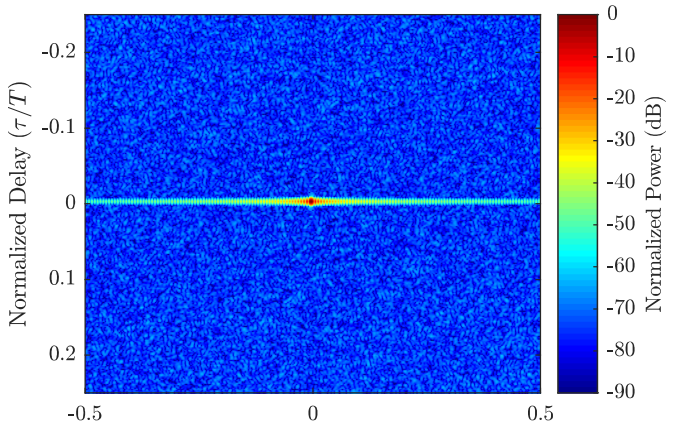


Fig. 3. MF PSF without spectral notch (without interference)

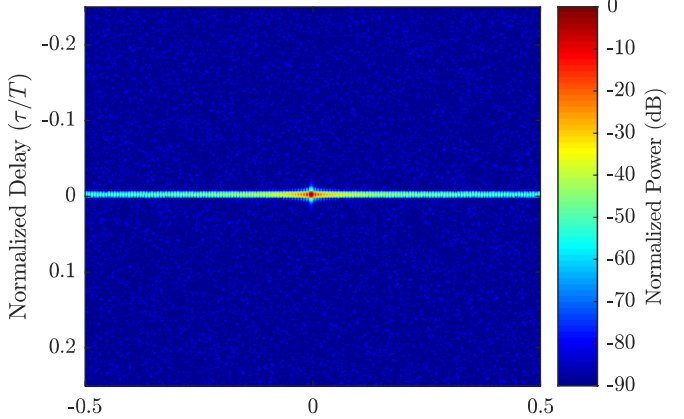


Fig. 4. LS-MMF PSF without spectral notch (without interference)

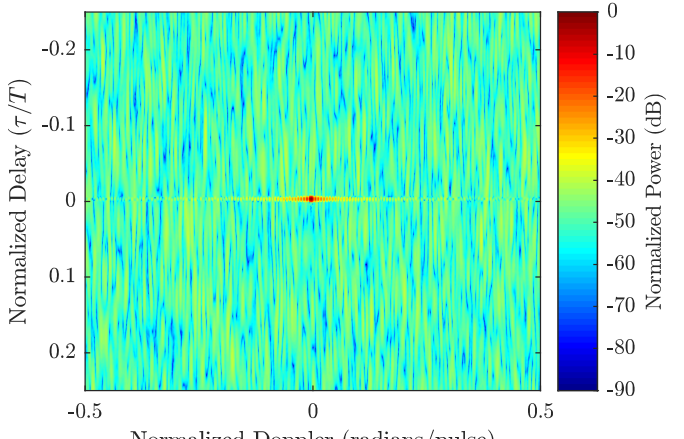


Fig. 5. Point spread function without a spectral notch and mismatched filtering with interference

B. Case 2: Stationary Spectral Notch

Figures 6 and 7 show the PSF resulting from the MF and LS-MMF, respectively, when a stationary spectral notch is formed. While the latter once again greatly reduces the background (in this case from -68.2 dB for the MF to -82.4 dB for the LS-MMF), we also observe the emergence of noticeable range sidelobes (the strong vertical response) at 0 Doppler. These sidelobes were not previously evident in Figs.

3 and 4 because the incoherent combining of FM noise waveform sidelobes during Doppler processing caused them to fade into the noise floor. Conversely, they are evident in Figs. 6 and 7 because even a tapered notch will experience some sidelobe increase (see [9]).

In terms of the metric in (4), these values for δ are roughly 1 dB and 3 dB higher than for Case 1. Examination of the figures reveals this increase to be predominantly driven by the spread immediately surrounding the 0 Doppler and 0 delay axes. The LS-MMF mismatch loss in this case has also increased somewhat to 1.4 dB.

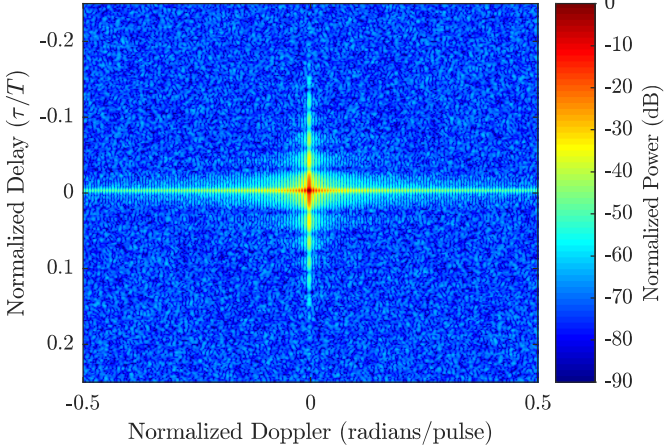


Fig. 6. Point spread function with a stationary spectral notch and matched filtering without interference

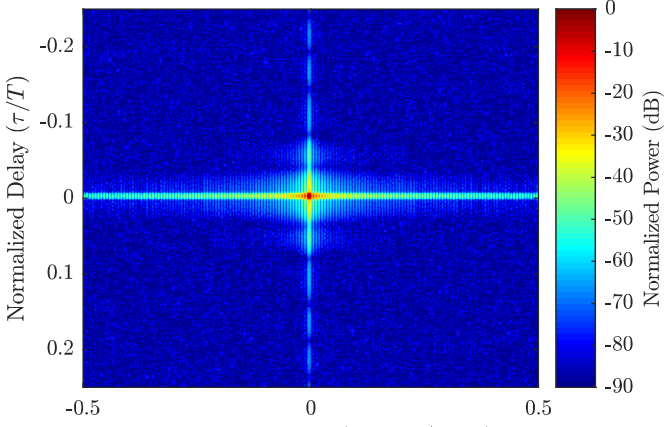


Fig. 7. Point spread function with a stationary spectral notch and mismatched filtering without interference

Figures 8 and 9 then show the PSF using MF and LS-MMF on the static notched waveforms when RFI is also present in the portion of the band covered by the notch. While transmit spectral notching reduces interference the radar causes to other users, the presence of the notch in each of the receive filters clearly reduces the degradation due to RFI caused to the radar.

In terms of the metric in (4) the background level is now found to be -66.9 dB and -73.9 dB for the MF and LS-MMF, respectively, which correspond to degradations relative to the RFI-free scenario of 1 dB and 8 dB. The greater degradation for the MMF arises from the shallower notch depth in Fig. 2 and the fact that the MMF response was better to start with.

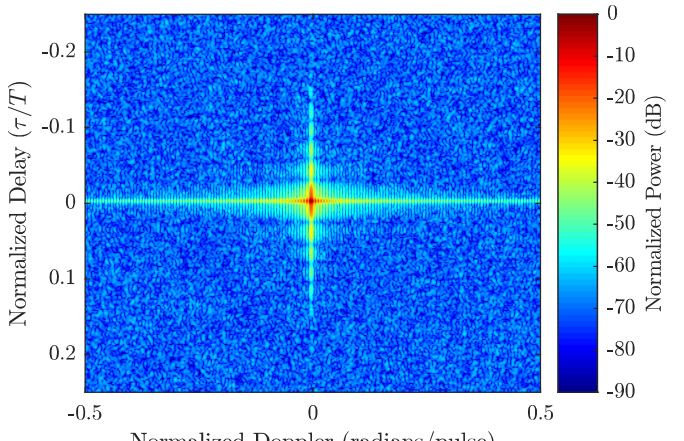


Fig. 8. Point spread function with a stationary spectral notch and matched filtering with interference

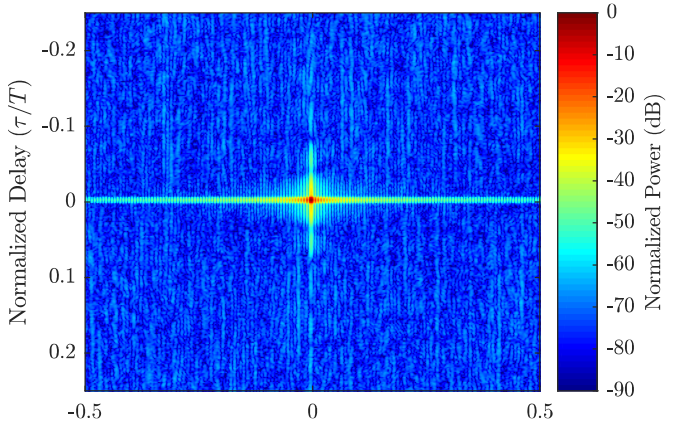


Fig. 9. Point spread function with a stationary spectral notch and mismatched filtering with interference

C. Case 3: Hopping Spectral Notch

Finally, Figs. 10 and 11 show the PSF for both filters when the notch location changes after every 10 pulses (thus 100 different locations during the 1000 pulse CPI). It is clear that excessive delay/Doppler spreading occurs in this case, though the LS-MMF is able to compensate for some of it. In terms of the background metric of (4), the MF and LS-MMF now realize -64.5 dB and -77.0 dB, respectively, which correspond to degradations of 4 dB and 5 dB relative to the stationary notch case (without RFI). The MMF also incurs a slightly greater mismatch loss here of 1.8 dB.

Figures 12 and 13 then depict the PSF for each filter when RFI is present. The metric of (4) has now increased to -63.8 dB and -71.6 dB for the MF and LS-MMF, respectively; an increase of 1 dB and 5 dB over the RFI-free scenario. The greater degradation for the MMF is again due to shallower filter notch depth and having more sensitivity to lose, though the MMF result still has an 8 dB advantage in addressing residual clutter from RSM when hopping RFI is present.

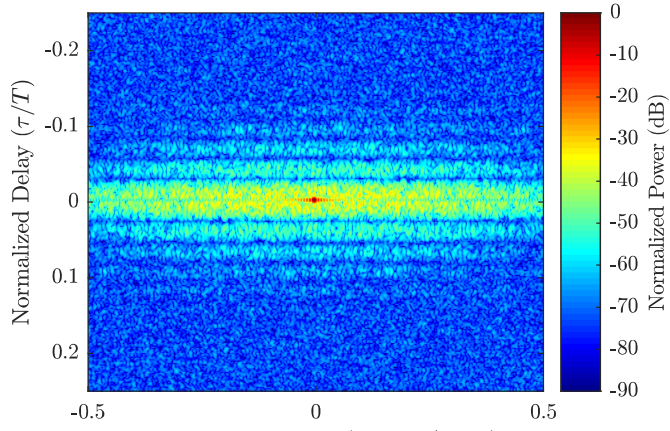


Fig. 10. Point spread function with a hopping spectral notch and matched filtering without interference

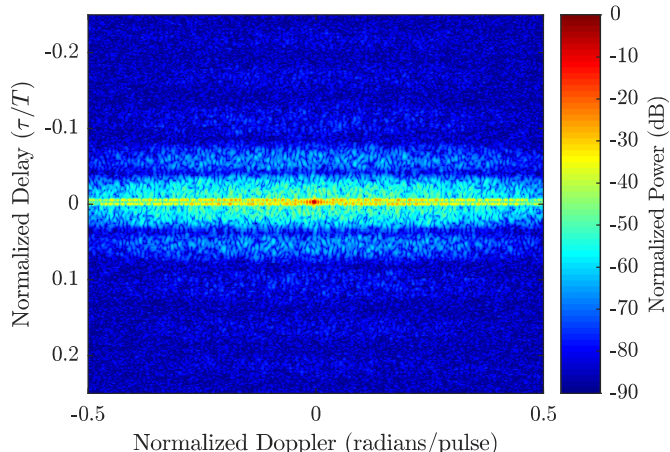


Fig. 11. Point spread function with a hopping spectral notch and mismatched filtering without interference

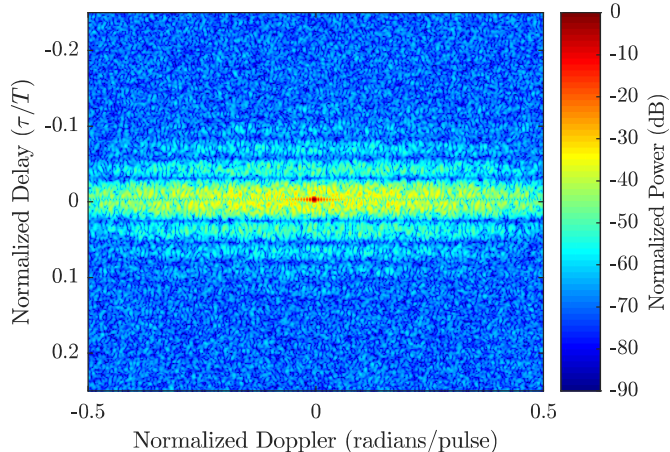


Fig. 12. Point spread function with a hopping spectral notch and matched filtering with interference

Table I summarizes the three cases for ease of comparison. It is interesting to note that at one extreme, where there is no spectral notch and no RFI, the MF realizes -69.5 dB. At the other extreme with hopping RFI present and a corresponding moving notch, the LS-MMF is still 2 dB better at -71.6 dB.

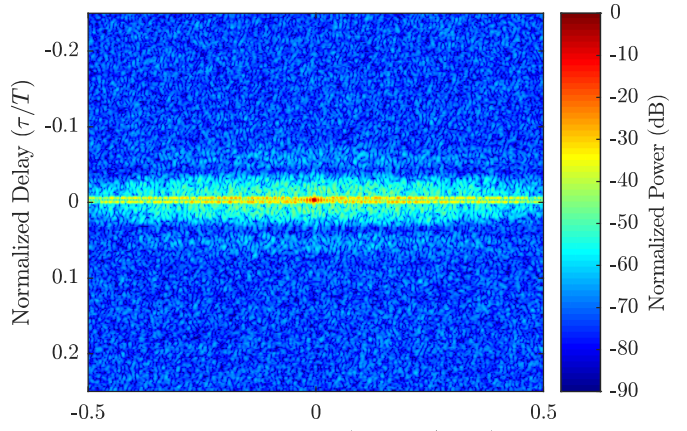


Fig. 13. Point spread function with a hopping spectral notch and mismatched filtering with interference

Table I. PSF metric from (4)

	δ (MF)	δ (LS-MMF)
No notch (w/o RFI)	-69.5 dB	-85.4 dB
No notch (with RFI)	-51.3 dB	-53.8 dB
Static notch (w/o RFI)	-68.2 dB	-82.4 dB
Static notch (with RFI)	-66.9 dB	-73.9 dB
Hopping notch (w/o RFI)	-64.5 dB	-77.0 dB
Hopping notch (with RFI)	-63.8 dB	-71.6 dB

V. EXPERIMENTAL ASSESSMENT OF LS-MMF

It is instructive to also consider how LS-MMF affects measured data. We use free-space measurements collected from the roof of Nichols Hall on the University of Kansas campus that illuminate moving targets within the intersection of 23rd & Iowa Streets in Lawrence, KS. A CPI of 2500 unique pulsed waveforms was transmitted and the echoes captured using the same system configuration as in [9], with the spectral notch moving after every 4th pulse.

Range-Doppler responses are formed by pulse compressing with either the MF or LS-MMF and then subsequently performing standard Doppler processing across the CPI. Since the platform is stationary, simple zero-Doppler projection clutter cancellation is employed. A Taylor window is applied to reduce Doppler sidelobes.

Figures 14 and 15 show the MF and LS-MMF range-Doppler responses, respectively. What is most readily apparent is that the streaking across Doppler has seemingly been sharpened in the process of modestly reducing sidelobes when LS-MMF is applied. In so doing, however, a number of false targets generated by the moving notches start to become visible (e.g. see range of 1030 meters around ± 20 m/s velocity).

This result implies that clutter RSM is actually not the only factor limiting performance when spectral notches move during the CPI. Preliminary indications are that these moving notches also modulate the pulse compression mainlobe, thereby requiring further compensation. A simple, yet rather effective approach [26] to address this phenomena has quite recently been developed and is still being explored.

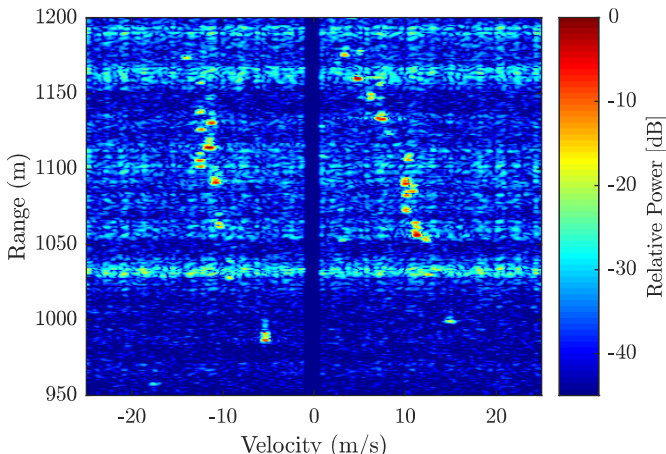


Fig. 14. Range-Doppler response with a hopping spectral notch and matched filtering without interference

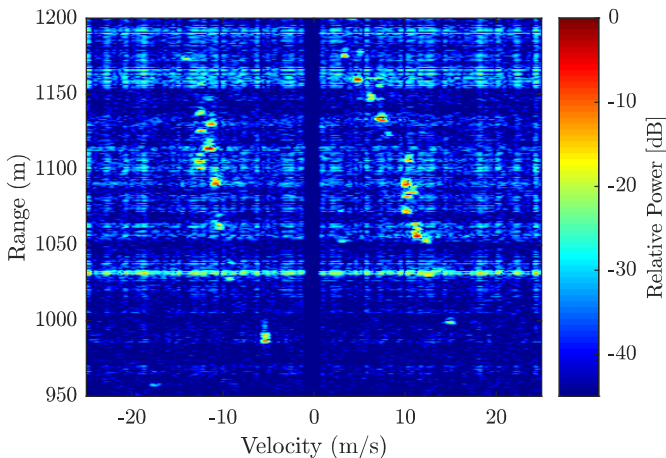


Fig. 15. Range-Doppler response with a hopping spectral notch and mismatched filtering without interference

CONCLUSIONS

It has been demonstrated using the delay/Doppler PSF that the LS-MMF provides an attractive alternative to the matched filter for spectrally notched waveforms, particularly when the notch location changes during the CPI to address dynamic RFI. The LS-MMF improves suppression of RSM that arises both from the normal variations between FM noise waveforms and the more extreme nonstationarity caused by hopping notch locations. The trade-offs for this improvement are a modest mismatch loss (less than 2 dB) and the attendant computational cost to obtain the filter. However, application of LS-MMF to free-space measurements shows that the residual clutter caused by the spectrally hopping notch is not solely an RSM effect, thereby necessitating additional means of compensation.

REFERENCES

- [1] H. Griffiths, L. Cohen, S. Watts, E. Mokole, C. Baker, M. Wicks, S. Blunt, "Radar spectrum engineering and management: technical and regulatory issues," *Proc. IEEE*, vol. 103, no. 1, pp. 85-102, Jan. 2015.
- [2] M. Labib, V. Marojevic, A.F. Martone, J.H. Reed, A.I. Zaghoul, "Coexistence between communications and radar systems – a survey," *URSI Radio Science Bulletin*, vol. 2017, no. 362, pp. 74-82, Sept. 2017.
- [3] J.M. Peha, "Sharing spectrum through spectrum policy reform and cognitive radio," *Proc. IEEE*, vol. 97, no. 4, pp. 708-719, Apr. 2009.
- [4] A.F. Martone, "Cognitive radar demystified," *URSI Bulletin*, no. 350, pp. 10-22, Sept. 2014.
- [5] P. Stinco, M.S. Greco, F. Gini, "Spectrum sensing and sharing for cognitive radars," *IET Radar, Sonar & Navigation*, vol. 10, no. 3, pp. 595-602, Feb. 2016.
- [6] A. Farina, A. DeMaio, S. Haykin, *The Impact of Cognition on Radar Technology*, IET, 2017.
- [7] B.H. Kirk, K.A. Gallagher, J.W. Owen, R.M. Narayanan, A.F. Martone, K.D. Sherbondy, "Cognitive software defined radar for time-varying RFI avoidance," *IEEE Radar Conf.*, Oklahoma City, OK, Apr. 2018.
- [8] B. Ravenscroft, S.D. Blunt, C. Allen, A. Martone, K. Sherbondy, "Analysis of spectral notching in FM noise radar using measured interference," *IET Intl. Conf. Radar Systems*, Belfast, UK, Oct. 2017.
- [9] B. Ravenscroft, J.W. Owen, J. Jakabosky, S.D. Blunt, A.F. Martone, K.D. Sherbondy, "Experiential demonstration and analysis of cognitive spectrum sensing and notching for radar," *IET Radar, Sonar & Navigation*, vol. 12, no. 12, pp. 1466-1475, Dec. 2018.
- [10] S.D. Blunt, E.S. Perrins, *Radar & Communication Spectrum Sharing*, IET, 2018.
- [11] A. Martone, K. Ranney, K. Sherbondy, K. Gallagher, S. Blunt, "Spectrum allocation for non-cooperative radar coexistence," *IEEE Trans. Aerospace & Electronic Systems*, vol. 54, no. 1, pp. 90-105, Feb. 2018.
- [12] J. Jakabosky, S.D. Blunt, B. Himed, "Spectral-shape optimized FM noise radar for pulse agility," *IEEE Radar Conf.*, Philadelphia, PA, May 2016.
- [13] S.W. Frost, B.D. Rigling, "Sidelobe predictions for spectrally-disjoint radar waveforms," *IEEE Radar Conf.*, Atlanta, GA, May 2012.
- [14] S.D. Blunt, M.R. Cook, J. Stiles, "Embedding information into radar emissions via waveform implementation," *Intl. Waveform Diversity & Design Conf.*, Niagara Falls, Canada, Aug. 2010.
- [15] T. Higgins, K. Gerlach, A.K. Shackelford, S.D. Blunt, "Non-identical multiple pulse compression and clutter cancellation," *IEEE Radar Conf.*, Kansas City, MO, May 2011.
- [16] C. Sahin, J. Jakabosky, P. McCormick, J. Metcalf, S. Blunt, "A novel approach for embedding communication symbols into physical radar waveforms," *IEEE Radar Conf.*, Seattle, WA, May 2017.
- [17] C. Sahin, J. Metcalf, S. Blunt, "Filter design to address range sidelobe modulation in transmit-encoded radar-embedded communications," *IEEE Radar Conf.*, Seattle, WA, May 2017.
- [18] M.H. Ackroyd, F. Ghani, "Optimum mismatched filters for sidelobe suppression," *IEEE Trans. Aerospace & Electronic Systems*, vol. AES-9, no. 2, pp. 214-218, Mar. 1973.
- [19] D. Henke, P. McCormick, S. D. Blunt, T. Higgins, "Practical aspects of optimal mismatch filtering and adaptive pulse compression for FM waveforms," *IEEE Radar Conf.*, Arlington, VA, May 2015.
- [20] C.A. Mohr, S.D. Blunt, "Analytical spectrum representation for physical waveform optimization requiring extreme fidelity," *IEEE Radar Conf.*, Boston, MA, Apr. 2019.
- [21] S. D. Blunt, M. Cook, J. Jakabosky, J. D. Graaf, E. Perrins, "Polyphase-coded FM (PCFM) radar waveforms, part I: implementation," *IEEE Trans. Aerospace & Electronic Systems*, vol. 50, no. 3, pp. 2218-2229, July 2014.
- [22] C.A. Mohr, P.M. McCormick, S.D. Blunt, "Optimized complementary waveform subsets within an FM noise radar CPI," *IEEE Radar Conf.*, Oklahoma City, OK, Apr. 2018.
- [23] C.A. Mohr, P.M. McCormick, S.D. Blunt, and C. Mott, "Spectrally-efficient FM noise radar waveforms optimized in the logarithmic domain," *IEEE Radar Conf.*, Oklahoma City, OK, Apr. 2018.
- [24] C.A. Mohr, S.D. Blunt, "FM noise waveforms optimized according to a temporal template error (TTE) metric," *IEEE Radar Conf.*, Boston, MA, Apr. 2019.
- [25] T. Higgins, T. Webster, A.K. Shackelford, "Mitigating interference via spatial and spectral nulling," *IET Radar, Sonar & Navigation*, vol. 8, no. 2, pp. 84-93, Feb. 2014.
- [26] J.W. Owen, B. Ravenscroft, S.D. Blunt, "Devoid clutter capture and filling (DeCCAF) to compensate for intra-CPI spectral notch variation," submitted to *SEE Intl. Radar Conf.*, Toulon, France, Sep. 2019.